Biology of Reproduction, 2023, **109(6)**, 864–877
https://doi.org/10.1093/biolre/ioad120
Advance access publication date 11 September 2023
Research Article

Segmental differentiation of the murine epididymis: identification of segment-specific, G_{M1}-enriched vesicles and regulation by luminal fluid factors†

Danielle M. Sosnicki[1,3,*], Roy Cohen[1,2], Atsushi Asano[4], Jacquelyn L. Nelson[1], Chinatsu Mukai[1], Pierre Comizzoli[3] and Alexander J. Travis[1,2]

[1]Cornell University, Baker Institute for Animal Health, Ithaca, NY, USA
[2]Cornell University, Department of Public and Ecosystem Health, Ithaca, NY, USA
[3]Smithsonian's National Zoo and Conservation Biology Institute, Department of Reproductive Sciences, Washington, DC, USA
[4]University of Tsukuba, Faculty of Life and Environmental Sciences, Tsukuba, Japan

***Correspondence:** Cornell University, Baker Institute for Animal Health, 235 Hungerford Hill Rd, Ithaca, NY 14853, USA. E-mail: dms552@cornell.edu

†**Grant Support:** This study was supported by funding from National Institutes of Health grant R01-HD093827 (AJT).

Abstract

The murine epididymis has 10 distinct segments that provide the opportunity to identify compartmentalized cell physiological mechanisms underlying sperm maturation. However, despite the essential role of the epididymis in reproduction, remarkably little is known about segment-specific functions of this organ. Here, we investigate the dramatic segmental localization of the ganglioside G_{M1}, a glycosphingolipid already known to play key roles in sperm capacitation and acrosome exocytosis. Frozen tissue sections of epididymides from adult mice were treated with the binding subunit of cholera toxin conjugated to AlexaFluor 488 to label G_{M1}. We report that G_{M1}-enriched vesicles were found exclusively in principal and clear cells of segment 2. These vesicles were also restricted to the lumen of segment 2 and did not appear to flow with the sperm into segment 3, within the limits of detection by confocal microscopy. Interestingly, this segment-specific presence was altered in several azoospermic mouse models and in wild-type mice after efferent duct ligation. These findings indicate that a lumicrine factor, itself dependent on spermatogenesis, controls this segmental differentiation. The RNA sequencing results confirmed global de-differentiation of the proximal epididymal segments in response to efferent duct ligation. Additionally, G_{M1} localization on the surface of the sperm head increased as sperm transit through segment 2 and have contact with the G_{M1}-enriched vesicles. This is the first report of segment-specific vesicles and their role in enriching sperm with G_{M1}, a glycosphingolipid known to be critical for sperm function, providing key insights into the segment-specific physiology and function of the epididymis.

Summary Sentence

The G_{M1}-enriched vesicles that transfer G_{M1} to the sperm plasma membrane during epididymal transit are highly abundant in segment 2 of the murine epididymis, and their differential presence is regulated by luminal fluid factors.

Graphical Abstract

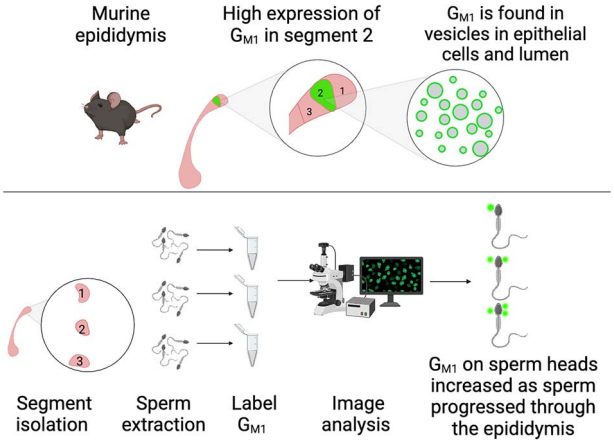

Key words: epididymis, sperm, ganglioside GM1, lumicrine signaling, efferent duct ligation, membrane raft

Received: June 19, 2023. **Revised:** August 17, 2023. **Accepted:** September 9, 2023

Introduction

Sperm are produced in the seminiferous tubules of the testis and then move into the rete testes from which they move into the efferent ducts. In the mouse, these ductules anastomose, forming a single tubule that turns into the initial segment of the epididymis [1–3]. The epididymis is a long, convoluted tubule that connects to the ductus deferens, which itself leads to the urethra and expels sperm and seminal fluid during ejaculation. Although sperm appear fully formed when leaving the testis, they must undergo specific consecutive biochemical changes during a maturational process in the epididymis. This maturation enables acquisition of motility and the ability to become fertilization-competent in the female tract during the process of capacitation [4–11]. Despite the fact that epididymal maturation is essential for physiologically relevant reproduction, we lack a complete understanding of this organ, particularly with regard to physiological/functional differences among the segments.

The murine epididymis can be separated into four broad regions: the initial segment, caput, corpus, and cauda. Each region is responsible for different general functions, from fluid resorption in the initial segment to sperm storage in the cauda. Rodent sperm also shed their residual cytoplasmic droplets during epididymal transit [12]. Within these broader regions of the organ, the mouse epididymis is naturally divided into 10 smaller segments that are well delineated by connective tissue septae [13, 14]. Based on previous descriptions of the structure of the mouse epididymis, segments 1–5 comprise the caput, segments 6–7 comprise the corpus, and segments 8–10 comprise the cauda (see Figure 1C) [13, 15]. The number of, and distinction between, segments varies widely among species [15–19] making the mouse an excellent model to look at sequential functions and processes. Gene expression in these segments is tightly regulated, with differential expression between segments being greater than the difference between some distinct organs, such as the liver and kidney [13]. For example, significant differences exist among segments in terms of their immunological environments and responses [20–23]. In addition to being androgen dependent, epididymal development and segmental differentiation have also been shown to depend on other factors produced by the testes that are released into the luminal fluid. When these lumicrine factors are removed, a number of changes occur in the epididymal tubule [4], including a de-differentiation of segments based on gene expression in the rat [24].

Sperm are transcriptionally and translationally silent as they transit through the epididymis [25, 26], and so, any changes in them are likely to be acquired through post-translational modifications or interaction with intraluminal factors. Epididymosomes are small membrane-bound extracellular vesicles (EVs) that have been implicated in some of the changes that sperm undergo during epididymal transit. They have been shown to transfer proteins, RNAs, lipids, and other factors to the sperm in multiple species, including the human and mouse [27–32]. The sperm plasma membrane also undergoes many changes during epididymal transit. Mouse sperm notably contain membrane raft domains that have a high proportion of cholesterol, sphingolipids, and glycosylphosphatidylinositol (GPI)-bound proteins [33]. Epididymosome membranes have similar composition, and rafts in sperm have been postulated to be binding sites for them [34, 35]. The exchange of lipids and protein materials with the sperm is one mechanism that could confer or change their functionality during epididymal transit [36–38].

The ganglioside G_{M1} is a sialic acid–containing glycosphingolipid that is primarily found in the outer leaflet of plasma membranes and can be found in many tissues but is most studied in the nervous system where it is relatively highly abundant. Gangliosides are known to participate in cell–cell recognition, adhesion, and signal transduction specifically within membrane raft domains [39]. Like other glycosphingolipids, gangliosides are primarily synthesized in the endoplasmic reticulum and modified in the Golgi apparatus by sequential addition of sugar moieties to a lipid backbone. This process is catalyzed by a series of specific glycosyltransferases, with five required for synthesis of G_{M1} [40]. The process begins with the ceramide backbone, and then, sugar residues are added onto the product of each previous step. The enzymes involved are ceramide glucosyltransferase (Glc-T), galactosyltransferase I (GalT-I), sialyltransferase I or G_{M3} synthase (ST-I), N-acetylgalactosaminyltransferase I or G_{M2}-synthase (GalNAc-T), and galactosyltransferase II or G_{M1}-synthase (GalT-II) [41].

We previously identified a novel mechanism of lipid regulation of calcium channels in sperm that, in turn, regulate acrosome exocytosis (AE) [42]. Both the removal of sterols and focal enrichments in G_{M1} can trigger calcium transients through the voltage-gated calcium channel $Ca_V2.3$, priming the sperm to undergo AE in response to calcium waves [42, 43]. The location of G_{M1} on the sperm head is conserved across mice, cattle, and humans [44, 45], and different patterns of G_{M1} localization in response to stimuli for capacitation have been found to be predictive of male fertility in humans [46, 47]. Knowing that this glycosphingolipid plays key roles in sperm function, we set out to better characterize its localization in the epididymis.

The objectives of this study were to (1) characterize the localization of G_{M1} in the murine epididymis, (2) determine the source and factors controlling G_{M1}-enriched vesicles observed in the epididymis, and (3) determine whether sperm were being enriched with G_{M1} during epididymal transit.

Here, we investigate a surprisingly dramatic segmental localization of G_{M1} in the murine epididymis and characterize its cell type and sub-cellular localization in vesicles. Through the use of mouse models that do not produce mature sperm and experiments involving efferent duct ligation (EDL), we demonstrate that this segmental localization is dependent upon a lumicrine factor that itself depends upon the presence of normal spermatogenesis in the testis. Furthermore, we confirm through differential gene expression analysis prior findings that loss of lumicrine factors results in global de-differentiation of the proximal epididymal segments. Lastly, we report that surface localization of G_{M1} on sperm increases as sperm transit from segment 2 to segment 3. Together, these data provide novel insights into segment-specific organization and function of the epididymis and sperm maturation in the epididymis.

Materials and methods

Reagents and animals

All reagents were purchased from Sigma unless otherwise noted. Wild-type C57BL/6 mice were bred onsite or obtained from The Jackson Laboratory (Bar Harbor, ME, USA).

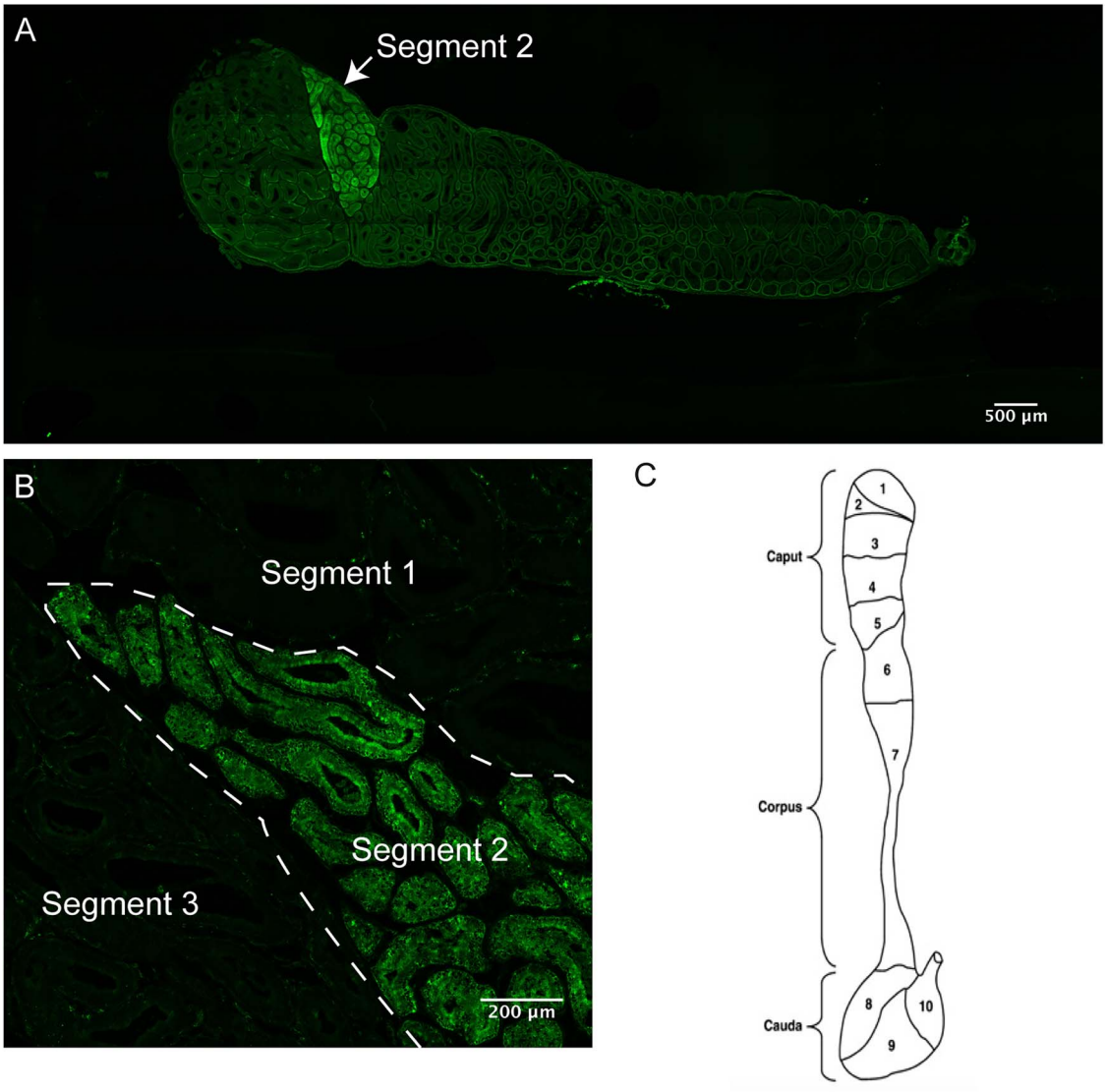

Figure 1. Segmental localization of G_{M1} in the murine epididymis. (A) Tissue section of the murine epididymis treated with CTB-488 to label G_{M1}, revealing enriched localization in segment 2. (B) Difference in CTB-488 fluorescence pattern between segments 1, 2, and 3 in the epididymis. (C) Diagram of segmental organization of the epididymis (adapted from Johnston et al., 2005) [13].

A knockout mouse model of MutS homolog 4 ($MSH4^{-/-}$) and a hypomorph mouse model of thyroid receptor interacting protein 13 ($Trip13^{gt/gt}$) were generous gifts from Dr. Paula Cohen and Dr. John Schimenti at Cornell University, respectively. All animal procedures were performed under the guidelines of the Institutional Animal Care and Use Committee at Cornell University (protocol 2002-0095).

Tissue handling for frozen tissue sections

Epididymides were obtained after euthanasia by cervical dislocation. Epididymides were dissected free of connective tissue, blood vessels, and fat and rinsed in phosphate-buffered saline (PBS). Tissues were blotted dry with KimWipes and allowed to equilibrate in Tissue-Tek OCT compound (Sakura Finetek USA, Torrance, CA, USA) for 5 min at room temperature in a small petri dish. Tissues were then blotted dry from excess OCT compound with a KimWipe and placed into plastic cryomolds and filled with fresh OCT compound. Molds were placed in a −80°C freezer overnight. No fixation or cryoprotective methods were performed on the tissues.

Tissue sections were cut on a Microm HM 50 5E cryostat set at −21°C at 5 μm thickness and thaw-mounted onto Fisher SuperFrost Plus charged slides (Fisher Scientific, Waltham, MA, USA). Slides were placed on a 37°C warm plate overnight and then immediately used for direct fluorescent labeling of G_{M1} or indirect immunofluorescence.

Direct fluorescent labeling of G_{M1} with cholera toxin

To label G_{M1}, cryosections were rehydrated with three washes of PBS, 5 min each. Tissue sections were outlined with a hydrophobic pen. The binding subunit of cholera toxin conjugated to Alexa Fluor 488 (CTB-488, Invitrogen Molecular Probes, Eugene, OR, USA) was reconstituted with PBS to a concentration of 1 mg/ml. CTB-488 was then diluted 1: 100 in PBS and applied to the rehydrated tissue sections for 1 h at room temperature, protected from light in a humid chamber. Next, the sections were washed three times with PBS, 5 min each and mounted with VectaShield antifade

mounting medium (Vector Laboratories, Burlingame, CA, USA).

Epididymal cell type markers

Tissue sections were rehydrated with three washes of PBS, 5 min each, and then blocked with 1% bovine serum albumin (BSA, w/v) in PBS for 30 min at room temperature. Primary antibodies that are specific for distinct epididymal cell types were diluted in 1% BSA blocking solution and applied to sections overnight at 4°C. For labeling principal cells, anti-Aquaporin 9 antibody (AQP-009, Alomone Labs, Jerusalem, Israel) was diluted at 1:100 [48, 49]; for basal cells, anti-cytokeratin 5 antibody (ab53121, abcam, Waltham, MA, USA) was diluted at 1:1000 [50, 51]; and for clear cells, anti-V-ATPase B1 antibody (PA5–101951, Invitrogen Life Technologies, Carlsbad, CA, USA) was diluted at 1:100 [52]. Sections were washed three times with PBS, 5 min each, and appropriate secondary antibodies were used at 1:200 dilutions for 1 h at room temperature. Slides were washed three times with PBS, and then, CTB-488 1:100 was applied as above. Slides were washed three times with PBS, 5 min each, and Hoechst was applied at 1:10 000 dilution for 5 min. Slides were washed three more times with PBS and mounted with VectaShield antifade medium.

Efferent duct ligation

The EDL procedures were performed on 8–10-week-old C57BL/6 mice under isoflurane anesthesia. A midline abdominal incision was made, and the testis, epididymis, and fat pad were externalized. Using a dissecting microscope, the efferent ducts were located and ligated with 4–0 PDS suture just before they entered segment 1 of the epididymis, with care to avoid ligating blood vessels. A sham procedure was performed on the contralateral epididymis of each animal that involved externalizing the testis, epididymis, and fat pad and locating the efferent ducts through the dissecting scope, but no ligation was performed. The incision was closed by suturing the abdominal wall (4–0 PDS), and then, tissue glue was applied to close the skin. The animals were treated with buprenorphine for analgesia and housed individually following the procedures. At 3 weeks post-EDL, animals were euthanized by cervical dislocation and epididymal tissue was collected and processed for direct fluorescence labeling of G_{M1} or for segment isolation for RNA extraction and sequencing.

Epididymal segment isolation

Mice were euthanized by cervical dislocation. Epididymides were immediately removed, and excess fat was trimmed using sharp dissection. They were placed in cold PBS on ice and then positioned and immobilized by pinning them with 1-in. 30-gage needles. The tunica covering the epididymis was removed using sharp dissection under a dissecting microscope. Once the tunica was removed, the epididymides were again placed in cold PBS and blunt dissection was used along the plane of the septae delineating the individual segments so the single tubule passing between segments could be visualized through the dissecting microscope. This portion of the tubule was then cut to separate the segments from one another. Segments used for RNA extraction were immediately placed in RNAlater solution and stored at 4°C for 24–48 h until RNA extraction was performed or were moved to −80°C for long-term storage. Segments used for sperm collection were immediately transferred to fresh PBS.

RNA extraction and sequencing

The RNA extraction was performed using TRI Reagent LS (Molecular Research Center, Inc., Cincinnati, OH, USA). The RNA sequencing was performed on samples of epididymal segments 1, 2, and 3 of the epididymis on control epididymides without EDL (C1, C2, C3) and 3 weeks after EDL (L1, L2, L3). Tissue samples of each epididymal segment were pooled from two mice during RNA extraction to increase RNA yield of each segment and to minimize variation between segment isolations and individual animals. A total of 12 pooled samples were sequenced, 2 from each segment and condition. Library preparation and sequencing were performed by the Transcriptional Regulation & Expression Facility at Cornell University in Ithaca, NY. Briefly, directional RNA-seq libraries were prepared from 500 ng total RNA using the NEBNext Directional Ultra II RNA Library Prep Kit for Illumina (New England Biolabs, Ipswich, MA, USA), with initial polyA+ isolation with the NEBNext Poly(A) mRNA Magnetic Isolation Module (New England Biolabs, Ipswich, MA, USA). Sequencing was performed on a NovaSeq 6000 (Illumina, Inc., San Diego, CA, USA) targeting 20 M raw reads per sample. Reads were trimmed for low quality and adaptor sequences, and mapped to the *Mus musculus* genome GRCm38/mm10. RNA extraction, library preparation, and sequencing were performed in two batches, each containing one replicate of each sample listed above.

Differential expression analysis

Differentially expressed genes (DEGs) analysis was performed on all data using the DESeq2 R package [53] controlling for batch (library preparation and sequencing run) and condition (ligated or control) to compare gene expression between combined segments 1, 2, and 3 without ligation (control, samples C1, C2, C3) and after EDL (ligated, samples L1, L2, L3). Separate analyses were performed to compare each individual non-ligated (control) segment with its ligated counterpart [i.e., segment 1 ligated (L1) compared to segment 1 control (C1)], by running DESeq2 and controlling for batch (library prep and sequencing) and group (C1, C2, C3, L1, L2, or L3) and then setting contrasts to compare L1 to C1, L2 to C2, and L3 to C3. DESeq2 provides statistical routines for determining differential expression in digital gene expression data by using a model based on a negative binominal distribution. The resulting *p*-values from the Wald test were adjusted using Benjamini and Hochberg's approach for controlling the false discovery rate [53]. Genes with absolute fold change $|\text{fc}| \geq 2$ and an adjusted *p*-value (*q*-value) < 0.05 as calculated by DESeq2 were considered differentially expressed.

Functional enrichment analysis using DAVID and enrichment map

The acquired DEG lists were filtered for protein coding genes and then analyzed for gene set enrichment with the DAVID [54, 55] tool using functional annotation databases of Gene Ontology and KEGG pathways and setting the species to *M. musculus*. Based on microscopy results that showed a shift in G_{M1} localization after EDL (a sharp decrease in G_{M1} localization in segment 2 and a modest increase in G_{M1} localization in segment 1), we analyzed lists of downregulated

DEGs in segment 2 and upregulated DEGs in segment 1. The EASE score (modified Fisher exact *p*-value of enrichment) was set to 0.1. A functional enrichment network was built based on DAVID output charts of gene-set enrichment genes that were upregulated in segment 1 and downregulated in segment 2 and filtered for terms that included "lipid" or "ganglioside" using the Enrichment Map [56] app in Cytoscape [57] (version 3.9.1).

G_{M1} quantification on sperm heads

Epididymal segments were isolated as described above from WT mice ($n = 9$ mice). To isolate sperm from the individual segments, each segment was individually minced in 500 μl PBS and sperm were allowed to seep out from the minced tissue for 15 min. The liquid was collected and centrifuged at 100× *g* for 1 min in a swinging bucket rotor in a 15 ml conical tube to pellet tissue debris. The supernatants containing the sperm were moved to 14 ml round-bottomed tubes, resuspended in an additional 500 μl PBS, and centrifuged at 400× *g* for 8 min to pellet sperm. A set volume of supernatant was carefully removed without disturbing the loose sperm pellet, leaving the sperm in 300 μl of PBS. The sperm pellet was resuspended in this remaining volume of PBS and 1 μl of CTB-488 (1 mg/ml) was added to the tube. The tube was incubated in a 37°C water bath and protected from light for 20 min before imaging on the Olympus FluoView 3000 microscope with the 100× objective ($n = 221$ sperm from segment 1; $n = 217$ sperm from segment 2; $n = 183$ sperm from segment 3). All sperm within a given experiment were imaged using the same objective and settings for laser power, gain, and zoom.

Analysis was performed using ImageJ by cropping each image to the smallest rectangle that included the sperm head. Integrated density of the cropped image was measured. A portion of the background visible in this cropped image was also measured for integrated density and then multiplied by the area of the image and subtracted from the original integrated density yielding a more accurate measurement of CTB-488 signal coming from each sperm head by removing the background signal that varied across images. These corrected integrated densities were then compared across the segments by performing one-way ANOVA.

Experiments examining the effects of 4 h incubation were performed by collecting sperm from individual segments as described above ($n = 5$ mice), immediately imaging aliquots of sperm from each segment after 20 min of incubation with CTB-488, and allowing the other half of the sperm sample to incubate in a modified Whitten medium (MW; 22 mM HEPES, 1.2 mM $MgCl_2$, 100 mM NaCl, 4.7 mM KCl, 1 mM pyruvic acid, 4.8 mM lactic acid hemi-Ca2+ salt, pH 7.35) [58] supplemented with 5.5 mM glucose. This is a non-capacitating medium as no mediators of sterol efflux were added for these experiments and was used to maintain sperm for 4 h at 37°C before they were incubated with CTB-488 for 20 min and then immediately imaged. Analysis was performed as described above, and the integrated density of the CTB-488 fluorescence between sperm isolated from one segment and sperm isolated from that same segment after 4 h of incubation was compared by using Student *t*-tests ($n = 125$ for segment 1 sperm with no incubation and $n = 116$ for segment 1 sperm after 4 h incubation; $n = 121$ for segment 2 sperm with no incubation and $n = 95$ for segment 2 sperm after 4 h incubation; and $n = 102$ for segment 3 sperm with no incubation and $n = 105$ for segment 3 sperm after 4 h incubation).

Image acquisition and image analysis

Imaging was performed on an Inverted Olympus FV3000 confocal microscope (Olympus, Center Valley, PA, USA). Multi-area tile scans were used to capture large areas of tissue sections and then stitched together using the Olympus FluoView 3000 software FV31S-SW (version 2.4.1.198). Integrated density measurements were performed in ImageJ [59] [version 1.51 (100)], and calculations were performed with Microsoft Excel (version 16.72).

Experimental design and statistical analysis

G_{M1} localization was examined in the epididymis of WT mice by labeling frozen tissue sections with CTB-488 ($n = 10$ mice). Frozen tissue sections of the epididymides of azoospermic mouse models ($n = 3$ mice) were labeled with CTB-488 to confirm that G_{M1} was present in the absence of sperm. The EDLs were performed on WT mice ($n = 11$ mice), and frozen tissue sections of the whole epididymis were made 1 week post-EDL ($n = 1$ mouse), 2 weeks post-EDL ($n = 1$ mouse), and 3 weeks post-EDL ($n = 5$ mice), and the remaining animals ($n = 4$ mice) were used for epididymal segment isolation for RNA extraction and sequencing 3 weeks post-EDL.

To quantify G_{M1} on sperm extracted from individual epididymal segments, first, segments 1, 2, and 3 were isolated from the epididymides of WT mice ($n = 9$ mice) and sperm were collected from each of the segments and then labeled with CTB-488. To assess whether passage of time had an effect on the amount of G_{M1} on the sperm from individual segments, epididymal segments were isolated from WT mice ($n = 5$ mice) and sperm were extracted and incubated for 4 h prior to CTB-488 labeling.

Statistical analysis to compare the quantity of G_{M1} on the heads of sperm collected from epididymal segments 1, 2, and 3 was performed using one-way ANOVA with multiple comparisons to compare segments 1 and 2, segments 1 and 3, and segments 2 and 3. Unpaired *t*-tests were used to compare one individual segment without and with a 4 h incubation. All statistical calculations were performed using GraphPad Prism (version 6 for Windows, La Jolla, CA, USA).

For this study, we use the term "vesicle" to describe the small G_{M1}-enriched structures observed via microscopy within epididymal epithelial cells and within the epididymal lumen that can interact with sperm.

Results

G_{M1} localization in the epididymis and factors controlling its localization

The G_{M1} was highly localized to segment 2 of the caput region of the mouse epididymis (Figure 1) and, as noted below, was also found in the efferent ductules. Within segment 2, G_{M1} was present in vesicles that were seen within the cells of the epithelium and in the lumen (Figure 2). The vesicles ranged in size up to 500 nm; limitations in resolution for confocal microscopy do not allow accurate detection or measurement of vesicles smaller than ~200 nm [60, 61]. Antibodies were used as cell markers for principal cells, clear cells, and basal cells (Figure 3). Anti-Aquaporin 9 (Figure 3A4) and anti-V-ATPase B1 (Figure 3B4) both labeled cells that were also

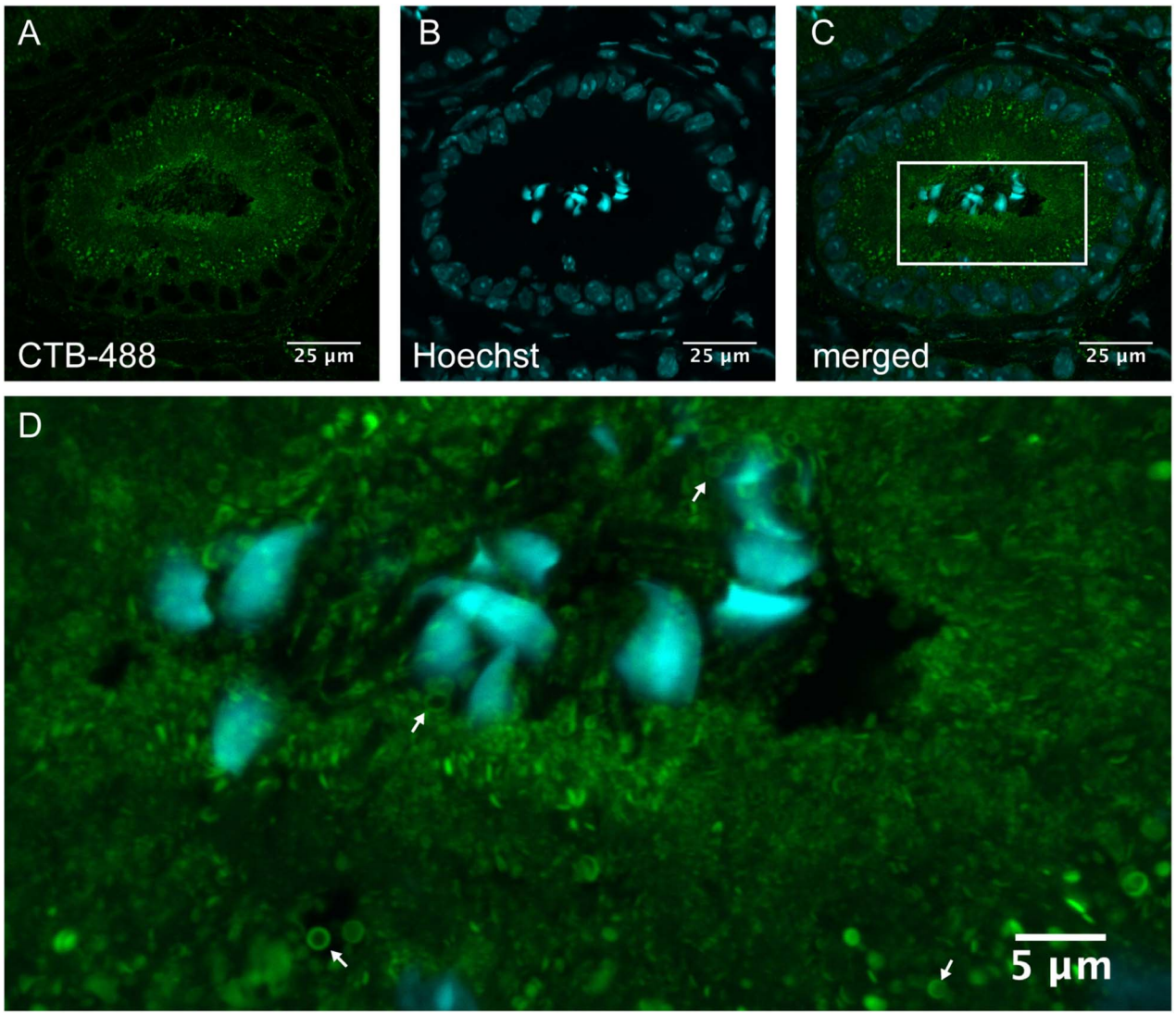

Figure 2. Detection of G_{M1}-enriched vesicles in a cross section of an epididymal tubule in segment 2. (A) CTB-488 was used to label G_{M1}-enriched vesicles. (B) Hoechst was used as a DNA stain. (C) Merged channels showing CTB-488 and Hoechst staining. (D) Magnified image of the rectangular inset in (C) that shows labeled G_{M1} in vesicles (arrows) within epithelial cells and in the lumen with sperm heads.

labeled with the CTB-488 signal, indicating that principal cells and clear cells produce or contain G_{M1}-enriched vesicles. Note that these antibodies show which types of cells contain the G_{M1}-enriched vesicles. We are not claiming co-localization between these markers and G_{M1} within these cells. Anti-keratin 5 labeled cells had no signal from CTB-488 (Figure 3C4), indicating that basal cells did not produce or contain G_{M1}-enriched vesicles.

To assess whether the G_{M1}-enriched vesicles could be originating from the sperm, such as cytoplasmic droplets that are shed from the sperm during epididymal transit, instead of the epididymal epithelium, we checked the G_{M1} localization in the epididymis of two different azoospermic mouse models (Figure 4). G_{M1} was still detected in the absence of sperm, but its localization in both azoospermic mouse models was altered from that in WT mice. The $MSH4^{-/-}$ mouse model (Figure 4A) had relatively high localization of G_{M1} in segment 2, although the segments in these mice were shaped differently than in WT mice; however, compared to WT, G_{M1} was not as sharply confined to one specific segment, and there was also increased labeling in adjacent segments 1 and 3 when compared to WT. The $Trip13^{gt/gt}$ mouse model (Figure 4B) had G_{M1} localization in a smaller area of the epididymis when compared to the $MSH4^{-/-}$ mouse, and most of the G_{M1} was localized to segment 1. The presence of G_{M1}-enriched vesicles in the epididymides of these models even in the absence of sperm in the lumen suggested that they were originating from the epididymal epithelium.

G_{M1} localization in the epididymis after EDL

To confirm that the vesicles were not originating from the testes and traveling in the luminal fluid apart from the sperm, and to determine whether the factor controlling G_{M1} localization in the epididymis was lumicrine or endocrine in nature, we performed EDLs on WT mice so that we could assess the G_{M1} localization in the epididymides of WT mice with fully functioning testes undergoing complete spermatogenesis, but without any sperm or luminal fluid factors entering the epididymis from the testis. Successful ligation was confirmed

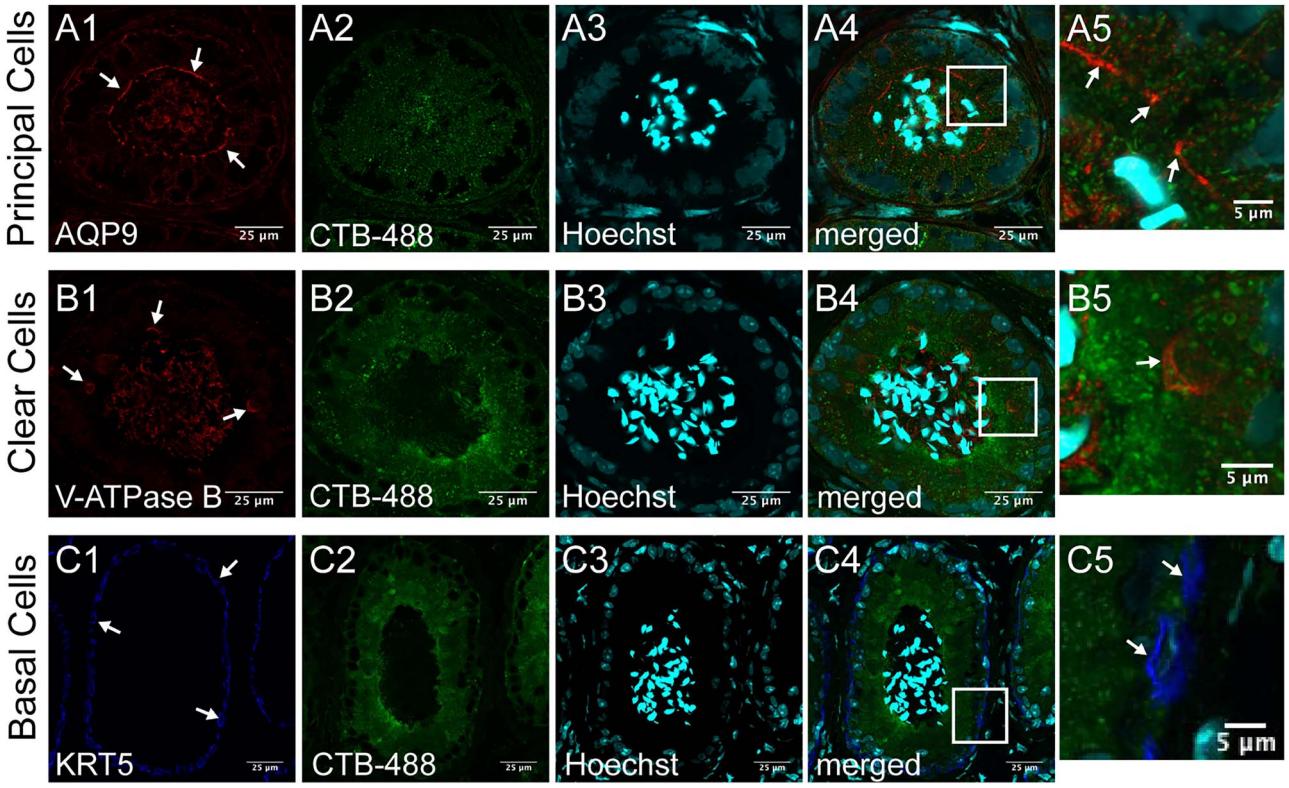

Figure 3. Cross sections of an epididymal tubule in segment 2. IIF was performed using antibodies for cell-specific marker (A1, B1, C1) cells with specific staining for each marker on select individual cells are shown with arrow; CTB-488 was used to label G_{M1}-enriched vesicles (A2, B2, C2); and Hoechst was used as a DNA stain (A3, B3, C3). Far right images (A5, B5, C5) are magnified images of the rectangular insets in the merged images (A4, B4, C4).

by microscopy via the lack of sperm in the epididymal lumen of the caput and proximal corpus on the frozen tissue sections. Additionally, it was noted that the ligated epididymis was smaller than the contralateral epididymis that only received the sham procedure. The tissue sections were labeled with CTB-488, and the control epididymis had consistent localization of G_{M1} in segment 2, as was seen in the WT mice without any procedures and was expected (Figure 4C). In contrast, the ligated epididymis of each animal showed altered G_{M1} localization (Figure 4D). Localization of G_{M1} was no longer confined to segment 2 of the epididymis, and instead, G_{M1} was detected more proximally, with increased localization in segment 1 of all mice observed.

RNA sequencing and differentially expressed genes analyses in the epididymis

Based on our microscopy results after EDL, we performed RNA sequencing to determine if we were seeing gene expression changes in segments 1–3 of the epididymis that could account for the change in G_{M1} localization. The RNA sequencing results showed a clear difference between control samples from segments 1, 2, and 3 of non-ligated epididymides indicating that segments were cleanly isolated with minimal contamination from adjacent segments. Principal component analysis (PCA; Figure 5) indicated that samples C1, C2, and C3, which were isolated from non-ligated epididymides, plotted more distinctly from one another, but samples L1, L2, and L3, which were isolated from ligated epididymides, clustered more closely together indicating that gene expression became more similar between segments after ligation was performed.

When comparing DEGs from ligated segments 1, 2, and 3 to control segments 1, 2, and 3, 1578 DEGs were identified (Supplementary Table S1). Of these, 1115 were protein coding genes (Supplementary Figure S1A). Of the protein coding genes, 922 were downregulated (ligated compared to control) and 193 were upregulated.

When comparing DEGs from ligated segment 1 to control segment 1, 4067 DEGs were identified (Supplementary Table S2). Of these, 3226 were protein coding genes (Supplementary Figure S1B). Of the protein coding genes, 1386 were downregulated (ligated compared to control) and 1804 were upregulated.

When comparing DEGs from ligated segment 2 to control segment 2, 1322 DEGs were identified (Supplementary Table S3). Of these, 1089 were protein coding genes (Supplementary Figure S1C). Of the protein coding genes, 770 were downregulated (ligated compared to control) and 319 were upregulated.

When comparing DEGs from ligated segment 3 to control segment 3, 395 DEGs were identified (Supplementary Table S4). Of these, 349 were protein coding genes (Supplementary Figure S1D). Of the protein coding genes, 305 were downregulated (ligated compared to control) and 44 were upregulated.

Functional enrichment analysis

To better attempt to determine the cause of the change in G_{M1} localization we observed via microscopy, we focused our functional analysis on the genes that were downregulated in segment 2 (where there was a decrease in G_{M1} localization) and genes that are upregulated in segment 1 (where there

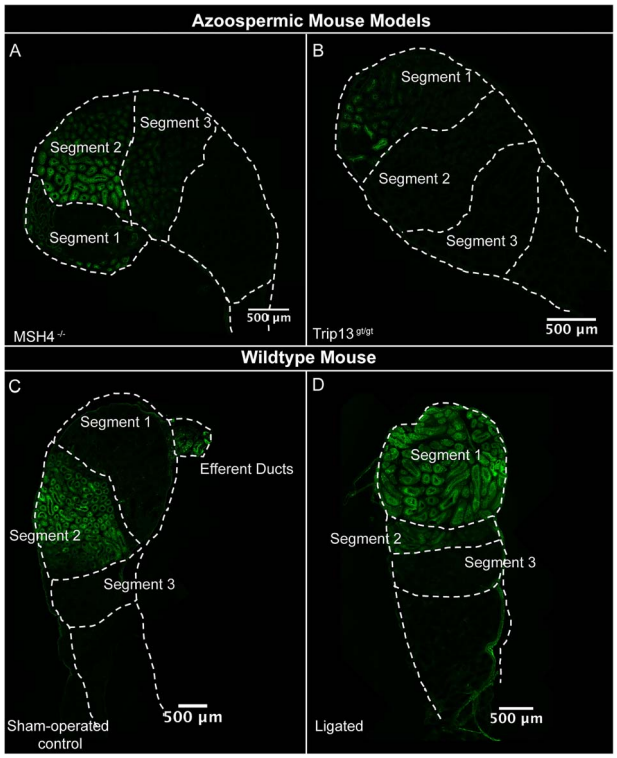

Figure 4. Tissue sections of the caput epididymis treated with CTB-488 to label G_{M1}. (A) G_{M1} localization in MSH4$^{-/-}$ azoospermic mouse. (B) G_{M1} localization in Trip13$^{gt/gt}$ azoospermic mouse model. (C) G_{M1} localization in non-ligated, sham-operated surgical control epididymis of WT mouse 3 weeks after surgery. (D) G_{M1} localization in the contralateral epididymis, which underwent EDL, 3 weeks after the surgical procedure.

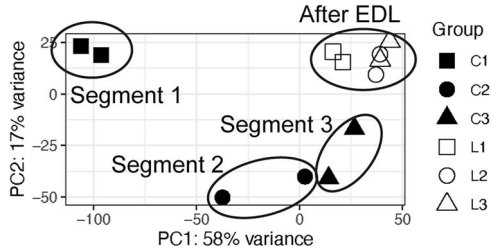

Figure 5. The PCA plot of RNAseq data from epididymal segments 1–3 after EDL (samples L1, L2, L3) and control segments (non-ligated) (samples C1, C2, C3). Results indicate a de-differentiation of the segments in response to EDL and are similar to previous findings in the rat by Turner et al [24].

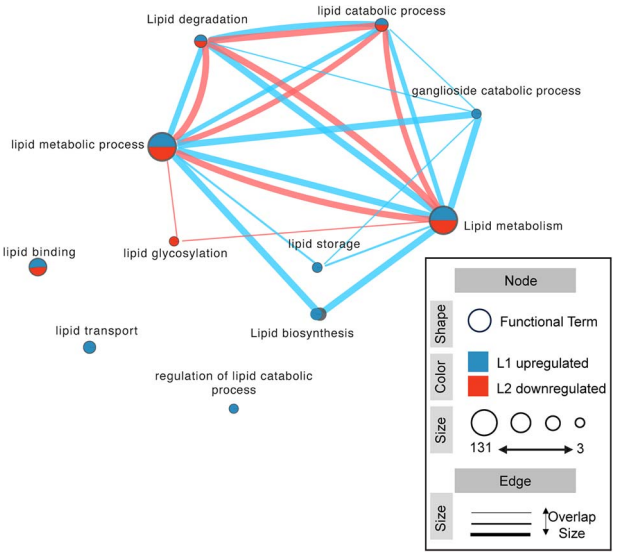

Figure 6. Large-scale changes in processes involving lipids based on differential expression of genes in response to EDL. Genes involved in processes that were upregulated in segment 1 are color-coded as blue nodes and lines connecting overlapping gene sets. Genes involved in processes that were downregulated in segment 2 after ligation are color-coded as red nodes and lines connecting overlapping gene sets. The node sizes are proportional to the number of genes that were in our dataset for each functional gene set term. Note the very broad impacts upon lipid biology in these segments upon loss of exposure to the lumicrine factor(s). Lipid biosynthesis increased overall in segment 1 after EDL, and genes involved in lipid glycosylation decreased in segment 2 after EDL.

was an increase in G_{M1} localization). Functional analysis in DAVID returned 22 annotation clusters based on the genes that were upregulated in segment 1 after ligation (Supplementary Table S5) and 13 annotation clusters based on the genes that were downregulated in segment 2 after ligation (Supplementary Table S6), indicating that there was a robust response to ligation and the removal of all lumicrine factors and sperm from the luminal environment of the epididymis. The network map produced by filtering for results that related to lipids and/or gangliosides (Figure 6) shows that many of the same processes that are downregulated in segment 2, as shown in red, are upregulated in segment 1, as shown in blue.

G_{M1} quantification on sperm heads

We hypothesized that these G_{M1}-enriched vesicles could be adding G_{M1} to the sperm during epididymal transit; therefore, we developed a method to quantify the G_{M1} on the sperm isolated from the segment having G_{M1}-enriched vesicles (segment 2), as well as the adjacent segments (segments 1 and 3) (Figure 7). There was a statistically significant increase of G_{M1} on sperm heads collected from segment 3 versus segment 1 ($p = 0.02$) and on sperm heads collected from segment 3 versus segment 2 ($p = 0.001$) (Figure 7D). Although these data reflected an increase in the amount of surface G_{M1} capable of being bound by CTB as sperm move spatially from segment 1 to segment 3, we also wanted to consider that there could be a temporal factor responsible for this increase; therefore, we incubated sperm isolated from each segment for a period of 4 h at 37°C to see whether there would be an increase in surface labeling of G_{M1}. After this incubation, we observed a significant increase in G_{M1} in sperm collected from segment 2 ($p = 0.02$) (Figure 7E). We also observed a significant increase in G_{M1} in sperm collected from segment 3 after incubation ($p = 0.02$). In contrast, we observed a decrease in G_{M1} between sperm from segment 1 and sperm from segment 1 after a 4 h incubation ($p = 0.02$) (Figure 7E).

Discussion

Our findings provide important new insights into segmental physiology and function of the epididymis and sperm maturation within the epididymis. We revealed that G_{M1} was highly localized in vesicles produced by epithelial cells in segment 2 of the mouse epididymis, that both this segmental localization and segmental differentiation based on gene expression in the caput epididymis as a whole were dependent on lumicrine

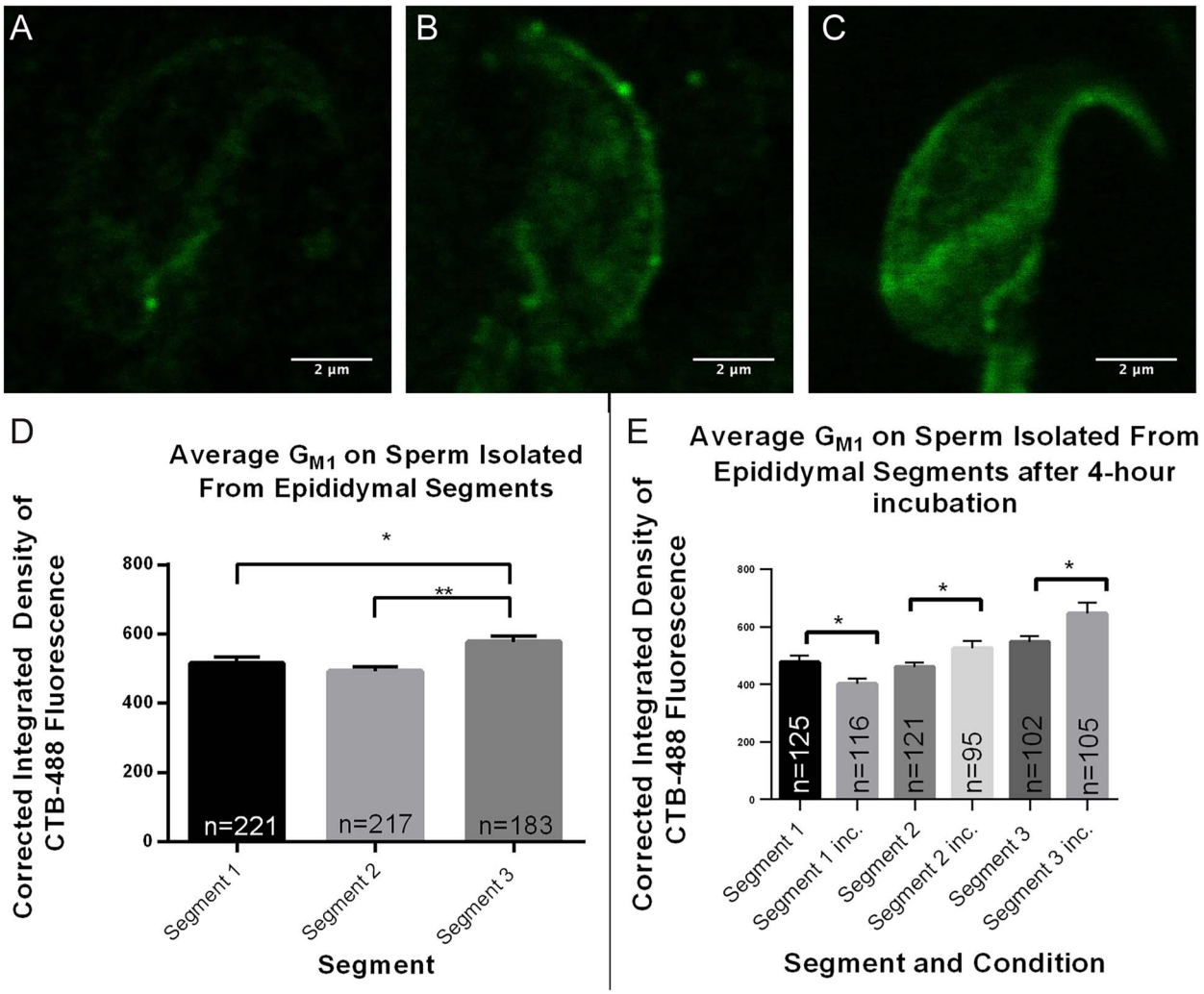

Figure 7. Representative images of CTB-488 labeling on sperm heads isolated from (A) segment 1, (B) segment 2, and (C) segment 3. For the purposes of quantification, integrated density of CTB-488 fluorescence was measured from images such as these, and used to (D) quantify the amount of G_{M1} present in the sperm heads from each segment. A one-way ANOVA was performed and showed a significant increase in G_{M1} after sperm transited through segment 2. Error bars show standard error of the mean. $*p < 0.05$, $**p < 0.01$. (E) CTB-488 fluorescence was used to quantify the amount of G_{M1} present on the sperm heads collected from each segment immediately after collection and after a 4 h incubation. T-tests were performed and showed a significant increase in G_{M1} after sperm incubation for segments 2 and 3 (after sperm were in segment 2) and a significant decrease after incubation in segment 1. Error bars show standard error of the mean. $*p < 0.05$.

signaling factors arising from testes supporting spermatogenesis and that these G_{M1}-enriched vesicles contributed to G_{M1} incorporation into the sperm during epididymal transit.

Using high-magnification confocal microscopy, we observed G_{M1}-enriched vesicles exclusively in principal cells, clear cells, and the lumen of segment 2. This finding is consistent with previous literature indicating that principal cells and clear cells in the caput are the primary cell types producing epididymosomes [62] and is also consistent with prior literature showing G_{M1} in membrane raft sub-domains of caput EVs in cattle, although segmental localization was not noted [63].

To determine whether the G_{M1}-enriched vesicles derived from the epididymal epithelium or from the sperm, possibly as shed cytoplasmic droplets, we first examined two different azoospermic mouse models. Epididymides from $Trip13^{gt/gt}$ mice [64] and $MSH4^{-/-}$ mice [65], which both contain genetic mutations that stop meiosis from reaching completion, both showed G_{M1} localization in the absence of mature sperm. However, the G_{M1} localization was altered compared to WT mice. Instead of being restricted to segment 2, we found that G_{M1} was localized in multiple segments in the $MSH4^{-/-}$ mice and with relatively increased localization in segment 1 in the $Trip13^{gt/gt}$ mice. Although these models showed that G_{M1} localization in the epididymis did not depend on the presence of mature sperm, they left open the question of whether the localization was under endocrine control, given that the androgen profiles of these mice have not been characterized. It has previously been suspected that inadequate crosstalk between developing male germ cells and Leydig cells can result in perturbations to normal androgen levels and behaviors [66]. Because these models were not undergoing complete spermatogenesis and their androgen profiles have not been fully assessed, we next wanted to evaluate whether the factor controlling G_{M1} localization was lumicrine or endocrine in nature. Therefore, we performed EDL on WT mice to keep the endocrine environment intact but remove potential lumicrine factors.

After EDL, we saw that the G_{M1}-enriched vesicles were still present in the absence of sperm, but the G_{M1} localization had again been altered, with G_{M1}-enriched vesicles in segments 1 and 2. These data are consistent with the presence of one or more lumicrine factors that are produced by a testis that supports complete spermatogenesis. Although it has been known for decades that lumicrine factors play a role in epididymal development, and it has been shown in the rat that removal of these lumicrine factors via EDL causes a de-differentiation to occur across segments [24], most lumicrine factors remain unidentified. In fact, the first testis-derived lumicrine factor was only recently identified in 2020 [67]. Although identification of the lumicrine factor at work here is beyond the scope of this set of studies, segmental G_{M1} localization provides an easily accessible marker of differentiation for those future studies. This finding also provides a new approach for isolation of segment-specific vesicles, as a step toward understanding segment-specific physiology. We hypothesize that these G_{M1}-enriched vesicles are a subpopulation of EVs, possibly epididymosomes, that originate from the epithelial cells lining segment 2 of the murine epididymis and aid in sperm maturation as sperm transit through segment 2 and are able to interact with them. In accordance with the guidelines of the International Society for Extracellular Vesicles (ISEV) [68], the term "extracellular vesicle" is preferred by the ISEV when an isolated sample has not been further analyzed for EV subtypes (i.e., exosome, microvesicle, etc.).

Gene expression changes in response to EDL

Our RNA sequencing results show many DEGs in each of the first three epididymal segments as a result of EDL, with many more being identified when the transcriptome changes are analyzed on a segmental level. The mouse epididymal transcriptome was previously reported using microarray analysis [13], and the effect of EDL on the proximal segments in the rat also based on microarray analysis was reported by the same group [24]. Our findings are the first report of the effect of EDL in the proximal segment of the mouse using next-generation sequencing and show a de-differentiation response similar to that reported in the rat after EDL [24]. Despite our current lack of complete understanding of epididymal regulation, it is clear that lumicrine factors play a substantial role in maintaining the distinct luminal milieus in each of the epididymal segments that are necessary for the sequential changes that are needed for proper sperm maturation. Our data show a larger impact (more DEGs) on segment 1 than on segment 2 and on segment 2 than on segment 3. These comparisons indicate that lumicrine factors may play an even larger role regulating the most proximal epididymal segments, compared to more distal ones.

Despite observing a substantial change in segmental localization of G_{M1} after EDL, the relative changes in RNA transcript expression associated with G_{M1} production did not rise to the top of the lists based on significance or enrichment. This finding suggests a global de-differentiation and not one specific to the production of gangliosides. To explore the cause of the change in G_{M1} localization, we focused our functional analysis on the gene set enrichment resulting from the genes that were downregulated in segment 2 and genes that are upregulated in segment 1 and filtered for terms related to lipids and gangliosides. From the network (Figure 6), it is evident that many of the processes have opposite gene regulation responses in segment 1 and segment 2, as evidenced by the nodes and connecting edges that appear red for gene sets that are based on downregulated gene lists from segment 2 and nodes and connecting edges that appear blue for gene sets that are upregulated in segment 1 (Figure 6).

The gene set within this filtered network that had the highest number of genes was "lipid metabolic process" with 131 input genes contributing to it. This indicates that there are many biological processes related to lipid metabolism that are being affected by EDL. Also noteworthy is the gene set for lipid biosynthesis, which is only enriched by upregulated genes in L1, as shown by the node and connecting edges only being blue (Figure 6). This shows that there is an increase of lipid synthesis occurring in segment 1 after ligation and may partially explain the increased localization of G_{M1} that we observe by microscopy and direct fluorescent labeling, although there are clearly many other lipid-related changes beyond the scope of G_{M1} localization that are occurring.

Ganglioside biosynthesis involves specific glycosyltransferases that transfer specific sugar residues to a proper lipid or oligosaccharide moiety. Of the genes responsible for the production of these transferases, only B4GALNT-1, which codes for G_{M2}-synthase, was differentially expressed in any of our segment comparisons. It was downregulated in L1 compared to C1, which is unexpected because L1 has an increased expression of G_{M1}-enriched vesicles. Because none of the other genes in the pathway were differentially expressed, the change in G_{M1} production/localization was likely due to some other perturbation of the system.

Cholera toxin preferentially binds to G_{M1} and does not have a strong affinity for other gangliosides [69]. It is possible that upregulation of neuraminidase expression led to cleaving off the sialic acid residue of G_{M1} thereby decreasing our ability to detect it using CTB-488. Of the four mammalian neuraminidases, only Neu1 and Neu2 were differentially expressed in our samples, unexpectedly being upregulated in L1. However, Neu3 has been shown to act most strongly on gangliosides [70], whereas Neu1 and Neu2 have other targets that we would not have observed changes in with our use of CTB-488.

Although our sequencing data did not pinpoint a specific perturbation of the G_{M1} synthesis pathway or a catabolic pathway to explain our observed response to EDL, the functional analysis results make clear that many genes related to lipid processes were regulated differentially. These findings suggest that screening for changes in other lipids/glycosphingolipids should be undertaken beyond G_{M1}, or the typical focus on proteins. It is also possible that although expression of specific genes in the G_{M1} synthetic pathway did not change, there were changes at the level of translation/protein abundance or other factors that modified the activity of the relevant enzymes; these are inherent limitations in interpreting the functional effects of changes in expression of specific RNA transcripts.

Increase in sperm surface G_{M1} by segment

Surface labeling of G_{M1} increased in sperm isolated from the spatial segments after they had completed passage through segment 2, the segment containing high concentrations of G_{M1}-enriched vesicles, and there was also an increase in surface labeling of G_{M1} after incubation of sperm that had entered or passed through segment 2. We hypothesize that one function of these vesicles may therefore be to enrich sperm in G_{M1} during epididymal transit. The increases from segments

1 to 3 and from 2 to 3 are consistent with our hypothesis that sperm are exposed to the G_{M1}-enriched vesicles upon entering segment 2 during their epididymal transit. These vesicles are then able to bind to the sperm plasma membrane and transfer the G_{M1}.

However, multiple alternative explanations for the increased surface labeling of G_{M1} exist and must be considered. The first could be that the G_{M1} was already present but was not properly oriented in the outer leaflet of the plasma membrane for CTB-488 to bind it. It has been reported that membrane cholesterol can induce a tilt in the glycolipid receptor headground that renders cholera toxin unable to bind to it [71]. This would be consistent with plasma membrane fluidity increasing as sperm transit through the epididymis [29]. However, our experiments comparing the amount of surface-labeled G_{M1} before and after a 4 h incubation showed significant increases in G_{M1} after incubation, and these were performed in a defined medium that did not include mediators of sterol efflux. Also, this increase in G_{M1} was not observed after incubation of sperm from segment 1, which had not yet been exposed to the G_{M1}-enriched vesicles present in segment 2.

The next alternative explanation for the increase in labeling upon incubation in vitro could be that the sperm from segment 1 were undergoing AE more than sperm from segments 2 or 3. To test this possibility, we performed Coomassie staining (data not shown) to assess whether sperm from each segment were undergoing AE during the 4 h incubation. We found that rates of spontaneous AE slightly increased as sperm moved from segment to segment, making any apparent increases in surface G_{M1} a conservative estimate and rendering this possible explanation unlikely.

Yet another alternative could be de novo synthesis of G_{M1} in the sperm. This is highly unlikely, as sperm lack the machinery (e.g., the endoplasmic reticulum), necessary to carry out this process. The next alternative mechanism is that G_{M1} could be present in internal stores of the sperm as they leave the testis and is being trafficked to the outer leaflet of the plasma membrane. Similarly, there is no evidence suggesting that there are intracellular vesicles moving between membranes within the sperm, such as between the acrosome and plasma membrane. Lastly, G_{M1} might not be present in internal stores, but might be associated with the inner leaflet. The action of floppases—enzymes that transport lipids from the inner to outer leaflet—could newly externalize G_{M1}. This mechanism cannot be ruled out by our current data, but is unlikely given that in most cells, G_{M1} associates with the outer leaflet of the plasma membrane and only faces inward in intracellular membranous structures directly involved in trafficking G_{M1} to the plasma membrane after it is synthesized in the endoplasmic reticulum or after endocytosing EVs.

Together, our findings suggest that G_{M1}-enriched vesicles transferred G_{M1} to the sperm. There is still much to learn about this interaction and transfer, which will be a focus for future studies. The first possible mechanism for transfer is that sperm could be endocytosing vesicles containing G_{M1}, and then trafficking G_{M1} to the sperm plasma membrane, similar to how other cell types might acquire vesicles containing G_{M1}. This is unlikely as sperm lack the endocytic machinery that would be necessary, and there is lack of evidence for any intracellular vesicles that would be capable of moving G_{M1} from one membrane to another.

Second, there could be some mechanism that allows for the CTB-488 to be able to bind G_{M1} on the sperm surface more efficiently. In one variation of this mechanism, contact with the vesicles might lead to changes in membrane fluidity and G_{M1} orientation as described above, enabling more binding with CTB. Another variation is that there could be an "unmasking" of G_{M1} that occurs during epididymal transit. It is known that components of seminal plasma are able to mask G_{M1} on ejaculated sperm [72], and there may be a component of testicular fluid that masks G_{M1} in a similar way but is removed during epididymal transit.

The third possible explanation, which we think the most likely, is that G_{M1} is being added to the sperm plasma membrane by G_{M1}-enriched EVs binding to the sperm surface and transferring G_{M1} directly to the plasma membrane via a transient fusion model, whereby small amounts of membrane from the EVs are transferred to the sperm plasma membrane. It is already known that EVs in the epididymis bind to sperm in this manner to transfer lipid, proteins, and microRNAs [29, 34, 73–75]. Additionally, G_{M1} is enriched in membrane raft domains, which may serve a targeting function [35], as well as binding sites, for the EVs. In this mechanism, G_{M1} facing inward in the EV, would, upon fusion, be facing the sperm cytoplasm and would reside on the inner leaflet. As the sperm restored membrane bilayer asymmetry through the actions of flippases, floppases, and/or scramblases, the G_{M1} would then move to the outer leaflet. This mechanism would be consistent with both the need for contact with the EVs in segment 2 and why after that contact, incubation in a defined medium with no lipid acceptors would result in an increase in outer leaflet localization.

Conclusions and future directions

To our knowledge, this is the first report of a possible subpopulation of epididymal vesicles (likely epididymosomes) originating from a single segment of the murine epididymis. Further characterizations of these vesicles enriched in G_{M1} at the lipidomic and proteomic levels, as well as studies on sperm membrane trafficking, will enhance our knowledge of epididymal segmental physiology and provide new insights into sperm maturation in the epididymis. Our gene expression data also provide important insights into lumicrine control of segmental differentiation and epididymal function. Together, this knowledge can lead to improved assisted reproductive technologies across taxa and help identify potential contraceptive targets.

Supplementary data

Supplementary data are available at *BIOLRE* online.

Acknowledgments

We thank and acknowledge the Transcriptional Regulation & Expression Facility of the Biotechnology Resource Center (RRID:SCR_022532) of Cornell Institute of Biotechnology for RNA sequencing, analysis, and support; Drs. Olga Amelkina and Jonathan Villanueva for their assistance with transcriptional functional analysis; Drs. Paula Cohen and John Schimenti for their generous gifts of the azoospermic mouse models; and Drs. Terry Turner and Daniel Johnston for their intellectual contributions and advice. This work was supported by National Institutes of Health grant R01-HD093827 (A.J.T), and

Cornell University's Baker Institute for Animal Health and College of Veterinary Medicine (A.J.T.).We would also like to acknowledge the Joint Graduate Training Program between Cornell University and Smithsonian's National Zoo and Conservation Biology Institute for support and training (D.M.S.). The graphical abstract was created with BioRender.

Conflict of interest

The authors have declared that no conflict of interest exists.

Authors' contributions

Conceived and designed experiments: DMS, AJT, RC, JLN, CM, and AA. Performed the experiments: DMS, JLN, CM, and AA. Analyzed the data: DMS and AJT. Manuscript preparation and critical discussion: DMS, AJT, RC, JLN, CM, and PC.

Data availability

The data discussed in this publication have been deposited in NCBI's Gene Expression Omnibus [76] and are accessible through GEO Series accession number GSE234995 (https://www.ncbi.nlm.nih.gov/geo/query/acc.cgi?acc=GSE234995).

References

1. James ER, Carrell DT, Aston KI, Jenkins TG, Yeste M, Salas-Huetos A. The role of the epididymis and the contribution of epididymosomes to mammalian reproduction. *Int J Mol Sci* 2020; **21**:5377.
2. Lambot M-AH, Mendive F, Laurent P, Schoore GV, Noël J-C, Vanderhaeghen P, Vassart G. Three-dimensional reconstruction of efferent ducts in wild-type and Lgr4 knock-out mice. *Anat Rec* 2009; **292**:595–603.
3. Nakata H, Iseki S. Three-dimensional structure of efferent and epididymal ducts in mice. *J Anat* 2019; **235**:271–280.
4. Robaire B, Hinton BT (eds.). *The Epididymis: From Molecules to Clinical Practice*. Boston, MA: Springer; 2002.
5. Turner TT. On the epididymis and its role in the development of the fertile ejaculate. *J Androl* 1995; **16**:292–298.
6. Hermo L, Robaire B. Epididymal Cell Types and Their Functions. In: Robaire B, Hinton BT (eds.), *The Epididymis: From Molecules to Clinical Practice*. Boston, MA: Springer; 2002: 81–102.
7. Cornwall GA. New insights into epididymal biology and function. *Hum Reprod Update* 2008; **15**:213–227.
8. Dacheux J-L, Dacheux F. New insights into epididymal function in relation to sperm maturation. *Reproduction* 2014; **147**:R27–R42.
9. Belleannee C, Belghazi M, Labas V, Teixeira-Gomes A-P, Gatti JL, Dacheux J-L, Dacheux F. Purification and identification of sperm surface proteins and changes during epididymal maturation. *Proteomics* 2011; **11**:1952–1964.
10. Skerget S, Rosenow MA, Petritis K, Karr TL. Sperm proteome maturation in the mouse epididymis. *PloS One* 2015; **10**:e0140650.
11. Barrachina F, Battistone MA, Castillo J, Mallofré C, Jodar M, Breton S, Oliva R. Sperm acquire epididymis-derived proteins through epididymosomes. *Hum Reprod* 2022; **37**:651–668.
12. Hermo L, Dworkin J, Oko R. Role of epithelial clear cells of the rat epididymis in the disposal of the contents of cytoplasmic droplets detached from spermatozoa. *Am J Anat* 1988; **183**:107–124.
13. Johnston DS, Jelinsky SA, Bang HJ, DiCandeloro P, Wilson E, Kopf GS, Turner TT. The mouse epididymal transcriptome: transcriptional profiling of segmental gene expression in the epididymis. *Biol Reprod* 2005; **73**:404–413.
14. Abou-Haïla A, Fain-Maurel MA. Regional differences of the proximal part of mouse epididymis: morphological and histochemical characterization. *Anat Rec* 1984; **209**:197–208.
15. Jelinsky SA, Turner TT, Bang HJ, Finger JN, Solarz MK, Wilson E, Brown EL, Kopf GS, Johnston DS. The rat epididymal transcriptome: comparison of segmental gene expression in the rat and mouse epididymides1. *Biol Reprod* 2007; **76**:561–570.
16. Domeniconi RF, Souza ACF, Xu B, Washington AM, Hinton BT. Is the epididymis a series of organs placed side by side? *Biol Reprod* 2016; **95**:10–10.
17. Turner TT, Johnston DS, Jelinsky SA, Tomsig JL, Finger JN. Segment boundaries of the adult rat epididymis limit interstitial signaling by potential paracrine factors and segments lose differential gene expression after efferent duct ligation. *Asian J Androl* 2007; **9**:565–573.
18. Kirchhoff C. The dog as a model to study human epididymal function at a molecular level. *Mol Hum Reprod* 2002; **8**:695–701.
19. Sullivan R, Mieusset R. The human epididymis: its function in sperm maturation. *Hum Reprod Update* 2016; **22**:574–587.
20. Pleuger C, Ai D, Hoppe ML, Winter LT, Bohnert D, Karl D, Guenther S, Epelman S, Kantores C, Fijak M, Ravens S, Middendorff R, *et al*. The regional distribution of resident immune cells shapes distinct immunological environments along the murine epididymis. *Elife* 2022; **11**:e82193.
21. Battistone MA, Mendelsohn AC, Spallanzani RG, Brown D, Nair AV, Breton S. Region-specific transcriptomic and functional signatures of mononuclear phagocytes in the epididymis. *Mol Hum Reprod* 2019; **26**:14–29.
22. Mendelsohn AC, Sanmarco LM, Spallanzani RG, Brown D, Quintana FJ, Breton S, Battistone MA. From initial segment to cauda: a regional characterization of mouse epididymal CD11c+ mononuclear phagocytes based on immune phenotype and function. *Am J Physiol Cell Physiol* 2020; **319**:C997–C1010.
23. Wijayarathna R, Pasalic A, Nicolas N, Biniwale S, Ravinthiran R, Genovese R, Muir JA, Loveland KL, Meinhardt A, Fijak M, Hedger MP. Region-specific immune responses to autoimmune epididymitis in the murine reproductive tract. *Cell Tissue Res* 2020; **381**:351–360.
24. Turner TT, Johnston DS, Finger JN, Jelinsky SA. Differential gene expression among the proximal segments of the rat epididymis is lost after efferent duct Ligation1. *Biol Reprod* 2007; **77**:165–171.
25. Kierszenbaum AL, Tres LL. Structural and transcriptional features of the mouse spermatid genome. *J Cell Biol* 1975; **65**:258–270.
26. Steger K. Transcriptional and translational regulation of gene expression in haploid spermatids. *Anat Embryol* 1999; **199**:471–487.
27. Sullivan R. Epididymosomes role of extracellular microvesicles in sperm maturation. *Front Biosci* 2016; **8**:106–114.
28. Sullivan R, Saez F. Epididymosomes, prostasomes, and liposomes: their roles in mammalian male reproductive physiology. *Reproduction* 2013; **146**:R21–R35.
29. Rejraji H, Sion B, Prensier G, Carreras M, Motta C, Frenoux J-M, Vericel E, Grizard G, Vernet P, Drevet JR. Lipid Remodeling of murine Epididymosomes and spermatozoa during Epididymal Maturation1. *Biol Reprod* 2006; **74**:1104–1113.
30. Rowlison T, Ottinger MA, Comizzoli P. Key factors enhancing sperm fertilizing ability are transferred from the epididymis to the spermatozoa via epididymosomes in the domestic cat model. *J Assist Reprod Genet* 2018; **35**:221–228.
31. Girouard J, Frenette G, Sullivan R. Comparative proteome and lipid profiles of bovine epididymosomes collected in the intraluminal compartment of the caput and cauda epididymidis: proteomic profiles of bovine epididymosomes. *Int J Androl* 2011; **34**:e475–e486.
32. Belleannée C. Extracellular microRNAs from the epididymis as potential mediators of cell-to-cell communication. *Asian J Androl* 2015; **17**:730–736.
33. Pike LJ. Rafts defined: a report on the keystone symposium on lipid rafts and cell function. *J Lipid Res* 2006; **47**:1597–1598.

34. Zhou W, Stanger SJ, Anderson AL, Bernstein IR, De Iuliis GN, McCluskey A, McLaughlin EA, Dun MD, Nixon B. Mechanisms of tethering and cargo transfer during epididymosome-sperm interactions. *BMC Biol* 2019; **17**:35.
35. Asano A, Selvaraj V, Buttke DE, Nelson JL, Green KM, Evans JE, Travis AJ. Biochemical characterization of membrane fractions in murine sperm: identification of three distinct sub-types of membrane rafts. *J Cell Physiol* 2009; **218**:537–548.
36. Choi YH, Toyoda Y. Cyclodextrin removes cholesterol from mouse sperm and induces capacitation in a protein-free medium. *Biol Reprod* 1998; **59**:1328–1333.
37. Davis BK. Influence of serum albumin on the fertilizing ability in vitro of rat spermatozoa. *Proc Soc Exp Biol Med* 1976; **151**: 240–242.
38. Visconti PE, Galantino-Homer H, Ning X, Moore GD, Valenzuela JP, Jorgez CJ, Alvarez JG, Kopf GS. Cholesterol efflux-mediated signal transduction in mammalian sperm. Beta-cyclodextrins initiate transmembrane signaling leading to an increase in protein tyrosine phosphorylation and capacitation. *J Biol Chem* 1999; **274**: 3235–3242.
39. Yu RK, Tsai Y-T, Ariga T. Functional roles of gangliosides in neurodevelopment–an overview of recent advances. *Neurochem Res* 2012; **37**:1230–1244.
40. Yu RK, Tsai Y-T, Ariga T, Yanagisawa M. Structures, biosynthesis, and functions of gangliosides—an overview. *J Oleo Sci* 2011; **60**: 537–544.
41. Yu RK, Ariga T, Yanagisawa M, Zeng G. Gangliosides in the Nervous System: Biosynthesis and Degradation. In: Fraser-Reid BO, Tatsuta K, Thiem J (eds.), *Glycoscience: Chemistry and Chemical Biology*. Berlin, Heidelberg: Springer; 2008: 1671–1695.
42. Cohen R, Buttke DE, Asano A, Mukai C, Nelson JL, Ren D, Miller RJ, Cohen-Kutner M, Atlas D, Travis AJ. Lipid modulation of calcium flux through CaV2.3 regulates acrosome exocytosis and fertilization. *Dev Cell* 2014; **28**:310–321.
43. Cohen R, Mukai C, Nelson JL, Zenilman SS, Sosnicki DM, Travis AJ. A genetically targeted sensor reveals spatial and temporal dynamics of acrosomal calcium and sperm acrosome exocytosis. *J Biol Chem* 2022; **298**:101868.
44. Selvaraj V, Buttke DE, Asano A, Mcelwee JL, Wolff CA, Nelson JL, Klaus AV, Hunnicutt GR, Travis AJ. GM1 dynamics as a marker for membrane changes associated with the process of capacitation in murine and bovine spermatozoa. *J Androl* 2007; **28**:588–599.
45. Buttke DE, Nelson JL, Schlegel PN, Hunnicutt GR, Travis AJ. Visualization of GM1 with cholera toxin B in live Epididymal versus ejaculated bull, mouse, and human Spermatozoa1. *Biol Reprod* 2006; **74**:889–895.
46. Cardona C, Neri QV, Simpson AJ, Moody MA, Ostermeier GC, Seaman EK, Paniza T, Rosenwaks Z, Palermo GD, Travis AJ. Localization patterns of the ganglioside GM1 in human sperm are indicative of male fertility and independent of traditional semen measures. *Mol Reprod Dev* 2017; **84**:423–435.
47. Moody MA, Cardona C, Simpson AJ, Smith TT, Travis AJ, Ostermeier GC. Validation of a laboratory-developed test of human sperm capacitation. *Mol Reprod Dev* 2017; **84**: 408–422.
48. Pastor-Soler N, Bagnis C, Sabolic I, Tyszkowski R, McKee M, Van Hoek A, Breton S, Brown D. Aquaporin 9 expression along the male reproductive tract. *Biol Reprod* 2001; **65**:384–393.
49. Elkjaer M, Vajda Z, Nejsum LN, Kwon T, Jensen UB, Amiry-Moghaddam M, Frøkiaer J, Nielsen S. Immunolocalization of AQP9 in liver, epididymis, testis, spleen, and brain. *Biochem Biophys Res Commun* 2000; **276**:1118–1128.
50. Shum WW, Smith TB, Cortez-Retamozo V, Grigoryeva LS, Roy JW, Hill E, Pittet MJ, Breton S, Da Silva N. Epithelial basal cells are distinct from dendritic cells and macrophages in the mouse epididymis. *Biol Reprod* 2014; **90**:90.
51. Kim SW, Kim B. Vacuolar H(+)-ATPase is not restricted to clear cells of the epididymal epithelium in cattle. *J Anim Sci Technol* 2021; **63**:262–271.
52. Belleannée C, Da Silva N, Shum WWC, Brown D, Breton S. Role of purinergic signaling pathways in V-ATPase recruitment to apical membrane of acidifying epididymal clear cells. *Am J Physiol Cell Physiol* 2010; **298**:C817–C830.
53. Love MI, Huber W, Anders S. Moderated estimation of fold change and dispersion for RNA-seq data with DESeq2. *Genome Biol* 2014; **15**:550.
54. Sherman BT, Hao M, Qiu J, Jiao X, Baseler MW, Lane HC, Imamichi T, Chang W. DAVID: a web server for functional enrichment analysis and functional annotation of gene lists (2021 update). *Nucleic Acids Res* 2022; **50**:W216–W221.
55. Huang DW, Sherman BT, Lempicki RA. Systematic and integrative analysis of large gene lists using DAVID bioinformatics resources. *Nat Protoc* 2009; **4**:44–57.
56. Merico D, Isserlin R, Stueker O, Emili A, Bader GD. Enrichment map: a network-based method for gene-set enrichment visualization and interpretation. *PloS One* 2010; **5**:e13984.
57. Shannon P, Markiel A, Ozier O, Baliga NS, Wang JT, Ramage D, Amin N, Schwikowski B, Ideker T. Cytoscape: a software environment for integrated models of biomolecular interaction networks. *Genome Res* 2003; **13**:2498–2504.
58. Travis AJ, Tutuncu L, Jorgez CJ, Ord TS, Jones BH, Kopf GS, Williams CJ. Requirements for glucose beyond sperm capacitation during in vitro fertilization in the mouse. *Biol Reprod* 2004; **71**: 139–145.
59. Schneider CA, Rasband WS, Eliceiri KW. NIH image to ImageJ: 25 years of image analysis. *Nat Methods* 2012; **9**:671–675.
60. Abbe E. Beiträge zur Theorie des Mikroskops und der mikroskopischen Wahrnehmung. *Archiv f mikrosk Anatomie* 1873; **9**:413–468.
61. Masters BR. *Superresolution Optical Microscopy: The Quest for Enhanced Resolution and Contrast*, vol. **227**. Cham: Springer International Publishing; 2020.
62. Rinaldi VD, Donnard E, Gellatly K, Rasmussen M, Kucukural A, Yukselen O, Garber M, Sharma U, Rando OJ. An atlas of cell types in the mouse epididymis and vas deferens. *Elife* 2020; **9**:9.
63. Girouard J, Frenette G, Sullivan R. Compartmentalization of proteins in Epididymosomes coordinates the Association of Epididymal Proteins with the different functional structures of bovine spermatozoa. *Biol Reprod* 2009; **80**:965–972.
64. Li X, Schimenti JC. Mouse Pachytene checkpoint 2 (Trip13) is required for completing meiotic recombination but not synapsis. *PLoS Genet* 2007; **3**:e130.
65. Kneitz B, Cohen PE, Avdievich E, Zhu L, Kane MF, Hou H, Kolodner RD, Kucherlapati R, Pollard JW, Edelmann W. MutS homolog 4 localization to meiotic chromosomes is required for chromosome pairing during meiosis in male and female mice. *Genes Dev* 2000; **14**:1085–1097.
66. Kim Y, Turner D, Nelson J, Dobrinski I, McEntee M, Travis AJ. Production of donor-derived sperm after spermatogonial stem cell transplantation in the dog. *Reproduction* 2008; **136**:823–831.
67. Kiyozumi D, Noda T, Yamaguchi R, Tobita T, Matsumura T, Shimada K, Kodani M, Kohda T, Fujihara Y, Ozawa M, Yu Z, Miklossy G, *et al.* NELL2-mediated lumicrine signaling through OVCH2 is required for male fertility. *Science* 2020; **368**: 1132–1135.
68. Théry C, Witwer KW, Aikawa E, Alcaraz MJ, Anderson JD, Andriantsitohaina R, Antoniou A, Arab T, Archer F, Atkin-Smith GK, Ayre DC, Bach J-M, *et al.* Minimal information for studies of extracellular vesicles 2018 (MISEV2018): a position statement of the International Society for Extracellular Vesicles and update of the MISEV2014 guidelines. *J Extracell Vesicles* 2018; **7**: 1535750.
69. Kuziemko GM, Stroh M, Stevens RC. Cholera toxin binding affinity and specificity for gangliosides determined by surface plasmon resonance. *Biochemistry* 1996; **35**:6375–6384.
70. Miyagi T, Yamaguchi K. Mammalian sialidases: physiological and pathological roles in cellular functions. *Glycobiology* 2012; **22**: 880–896.

71. Lingwood D, Binnington B, Róg T, Vattulainen I, Grzybek M, Coskun Ü, Lingwood CA, Simons K. Cholesterol modulates glycolipid conformation and receptor activity. *Nat Chem Biol* 2011; **7**:260–262.
72. Kawano N, Yoshida K, Iwamoto T, Yoshida M. Ganglioside GM1 mediates Decapacitation effects of SVS2 on murine spermatozoa. *Biol Reprod* 2008; **79**:1153–1159.
73. Belleannée C, Calvo É, Caballero J, Sullivan R. Epididymosomes convey different repertoires of MicroRNAs throughout the bovine Epididymis1. *Biol Reprod* 2013; **89**:30.
74. Sullivan R, Frenette G, Girouard J. Epididymosomes are involved in the acquisition of new sperm proteins during epididymal transit. *Asian J Androl* 2007; **9**:483–491.
75. Foot NJ, Kumar S. The Role of Extracellular Vesicles in Sperm Function and Male Fertility. In: Mathivanan S, Fonseka P, Nedeva C, Atukorala I (eds.), *New Frontiers: Extracellular Vesicles*. Cham: Springer International Publishing; 2021: 483–500.
76. Edgar R, Domrachev M, Lash AE. Gene expression omnibus: NCBI gene expression and hybridization array data repository. *Nucleic Acids Res* 2002; **30**:207–210.